Electr Eng (2017) 99:1065–1072
DOI 10.1007/s00202-016-0479-x

ORIGINAL PAPER

Effect of power factor on torque capability of FOC induction machine in field weakening region for propulsion systems

G. K. Nisha[1] · **Z. V. Lakaparampil**[2] · **S. Ushakumari**[3]

Received: 1 August 2016 / Accepted: 4 November 2016 / Published online: 14 November 2016

Abstract Propulsion system used in applications like electric traction, rolling stock, etc. requires high torque at low speed for starting and climbing and nearly constant power at high speed. Induction machines, which are rugged, reliable, low cost and has less maintenance, satisfy the characteristics of the propulsion and reinstating the traditionally used DC series motor for this purpose. Field oriented control (FOC) of induction machines can decouple its torque control from field control and extended speed range operation with constant power beyond rated speed by field weakening (FW). It is desirable to retain maximum torque capability in the FW region for propulsion applications at high speed. To produce maximum torque that machine could possibly develop at FW region, the maximum inverter voltage and current must be appropriately utilized. This paper proposes an innovative approach to improve the torque capability of induction machine in FW region by modifying the design of induction machine to change the bahaviour of the machine to suit propulsion requirements. Extensive simulation of the design options generated from the design modification has been carried out using MATLAB/Simulink and torque-speed characteristics are compared.

✉ G. K. Nisha
nishacharu@gmail.com

Z. V. Lakaparampil
zvlakapara@gmail.com

S. Ushakumari
ushalal2002@gmail.com

[1] Mar Baselios College of Engineering and Technology, Trivandrum, India

[2] Centre for Development of Advanced Computing (C-DAC), Trivandrum, Kerala, India

[3] Department of Electrical Engineering, College of Engineering Trivandrum, Trivandrum, India

Keywords Field oriented control · Space vector modulation · Field weakening · Induction machine · Propulsion

1 Introduction

Recent advancement in power electronics, microprocessor revolution and several new control technologies, such as vector and direct torque controls made it possible to replace DC machines with induction motors in applications like propulsion [1]. Induction motors are considered as a better choice for propulsion applications due to their robustness, reliability, and low cost.

The scalar control strategy for induction motor provides good steady state but poor dynamic response due to the deviation in the air gap flux linkage values [2]. The scalar control uses particular voltage and frequency for the control rather than its phase which results in the deviation of phase and magnitude values of the air gap flux linkages. These undesirable deviations may affect high performance of electric propulsion drives. Therefore, a high precision fast positioning speed control is required. A coordinated control of stator current magnitude, frequency and phase, makes induction motor drive a complex control. If the rotor flux linkages are resolved then the control of an induction motor becomes very similar to a separately excited DC machine.

In propulsion purpose, the induction motor has to operate at speeds higher than the rated one, which is achieved by field (flux) weakening. During the past two decades, several research papers were presented to achieve the maximum torque capability of the machine in the FW region and suggested various approaches [3–10]. The FW approaches can be categorized as: (1) variation of stator flux in inverse proportion to the rotor speed ($1/\omega_r$); (2) feed forward reference

flux generation on machine equations or machine models and (3) closed loop control of the stator voltage or voltage detection model.

The first approach as presented in [4], which is the most frequently used one in FW control, the flux is established inversely proportional to the motor speed. The method cannot produce maximum output torque for the available current nor the full utilization of DC-link voltage.

The second approach, as presented in [5], relies on the nonlinear equations of machine model and the constraints of voltage and current, which makes it parameter dependent. Thus the method can provide accurate results only if magnetic saturation is considered with known machine parameters of sufficient accuracy.

The third approach as described in [6–10], maximum available inverter voltage is utilized to produce maximum torque in FW region when the excitation level is adjusted by closed loop control of the machine voltage. Although it is not dependent on motor parameters and DC link voltage, demands an additional outer loop which is to be tuned and requires intensive computation. Also, the maximum torque is not generated in the upper portion compared to lower portion of the FW region.

In most of the approaches, maximum available inverter voltage is utilized to produce maximum torque in FW region when the excitation level is adjusted by closed loop control of the machine voltage. Field weakening has to be done without violating either current limit or voltage limit in such a manner that accelerating torque follows maximum torque trajectory. Most commonly used methods of excitation control do not fully utilize the installed inverter power which causes a reduction of torque and power down to 65% [11]. Alternative methods are needed to produce the maximum torque that the induction motor could possibly develop at FW region.

In this paper, a control strategy is developed for SVM inverter fed induction motor based on FOC scheme in FW region. A novel idea is proposed to improve the torque capability in FW region by design modification of the induction motor. The torque-speed characteristics of various design options are evaluated and compared by generating simulation results using MATLAB/Simulink. The paper is organized as follows: in the first section, the mathematical model and FOC of induction motor is reviewed. In the next sections, implementation of SVM inverter with FOC and the FW control of induction machine are presented. Then, the design modification and design options are proposed. Finally, simulation results and discussions are presented.

2 Field oriented control of induction machine

Field oriented control of induction machine can decouple its torque control from field control to give dynamic performance comparable to the separately excited DC motor. Independent control of motor flux and torque can be obtained by this method and it is possible by connecting coordinate system with rotor flux vector [11]. Figures 1 and 2 show the stator current space vector and equivalent circuit, respectively, of an induction motor.

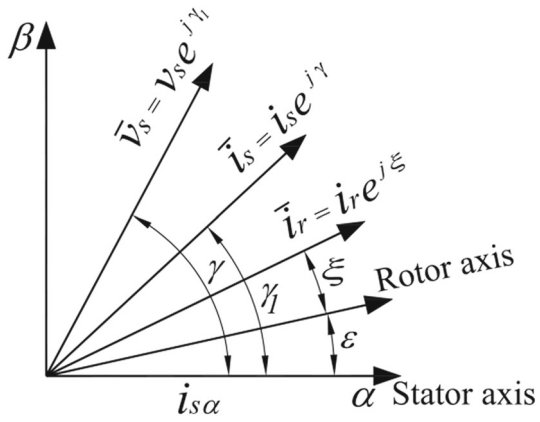

Fig. 1 Stator current space vector

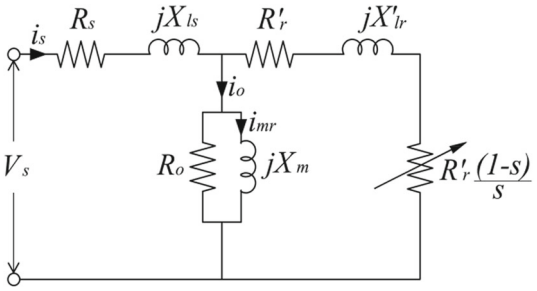

Fig. 2 Equivalent circuit of induction motor

Induction motor model equation in d–q reference frame is written as follows:

$$\vec{V}_s(t)e^{-j\theta} = R_s \vec{i}\, e^{-j\theta} + L_s \frac{d\vec{i}_s}{dt} e^{-j\theta} + L_m \frac{d(\vec{i}_r e^{j\varepsilon})}{dt} e^{-j\theta} \tag{1}$$

$$0 = R_r \vec{i}_r e^{j(\varepsilon-\theta)} + L_r \frac{d\vec{i}_r}{dt} e^{j(\varepsilon-\theta)} + L_m \frac{d(\vec{i}_s e^{-j\varepsilon})}{dt} e^{j(\varepsilon-\theta)} \tag{2}$$

$$\frac{d\omega_r}{dt} = \frac{T_d(t) - T_L(t)}{J} = \frac{1}{J}\left(\frac{2}{3}\frac{P}{2}\frac{L_m}{L_r}\left(\psi_{rd} i_{sq} - \psi_{rq} i_{sd}\right) - T_L\right), \tag{3}$$

where L_s stator self inductance; L_m magnetizing inductance; L_r rotor self inductance; R_s stator resistance; R_r rotor resistance; T_d electromagnetic torque; ω_r rotor speed; P number

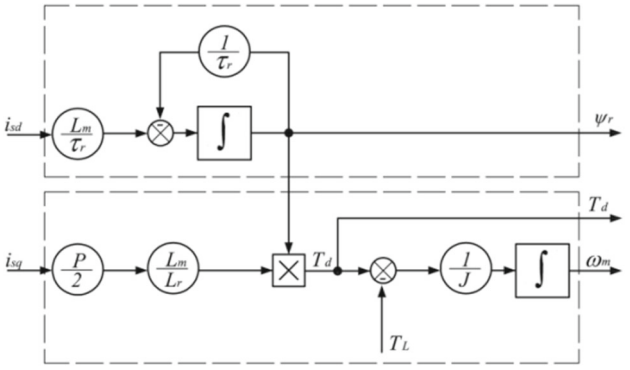

Fig. 3 Block diagram of induction machine in d–q coordinate system

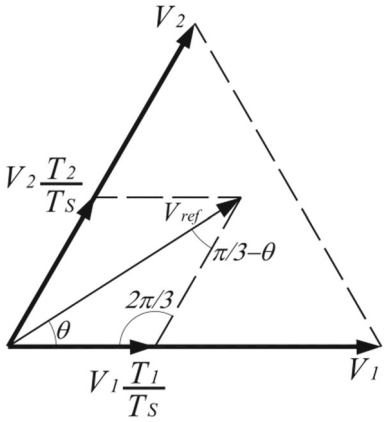

Fig. 4 Reference vector as a geometric summation of two nearest space vectors

of poles, J moment of inertia; i_{sd} stator d-axis current;i_{sq} stator q-axis current, ψ_{rd} rotor d-axis flux linkage; ψ_{rq} rotor q-axis flux linkage.

The block diagram of induction machine in d–q coordinate system is shown in Fig. 3. Up to the rated speed rotor magnetizing current is kept constant to get the fast control over electromagnetic torque of the machine because the dynamics of the magnetizing current involves a large time constant [12]. The magnetizing current is responsible for the magnetizing flux generation.

From the voltage loop equation the magnetizing current dependency on the d component of stator current is obtained as:

$$\frac{\mathrm{d}\psi_{\mathrm{rd}}}{\mathrm{d}t} + R_{\mathrm{r}} i_{\mathrm{rd}} = 0, \tag{4}$$

where i_{rd} rotor d-axis current; ψ_{rd} rotor d-axis flux linkage.

The two phase d–q model of an induction machine rotating at a speed will give the decoupled control concept [13]. To determine the rotor flux angle, first we need to calculate the slip speed using the following equation:

$$\omega_{\mathrm{slip}} = \frac{L_{\mathrm{m}}}{\tau_{\mathrm{r}}} \frac{i_{\mathrm{sq}}}{\psi_{\mathrm{rd}}} = \frac{1}{\tau_{\mathrm{r}}} \frac{i_{\mathrm{sq}}}{i_{\mathrm{mr}}}, \tag{5}$$

where i_{mr} rotor magnetizing current; τ_{r} rotor time constant; i_{sq} rotor q-axis current; ψ_{rq} rotor q-axis flux linkage.

3 SVM-based inverter

The transition of reference vector moving from one sector in the space vector diagram to the next requires minimum number of switching to reduce the switching losses. The six active vectors are of equal magnitude and are mutually phase displaced by $\pi/3$. These vectors divide the complex plane into the six sectors 1–6 [14]. Any desired reference voltage vector within the hexagon can be synthesized by decomposing it into components which lie along the active voltage vectors.

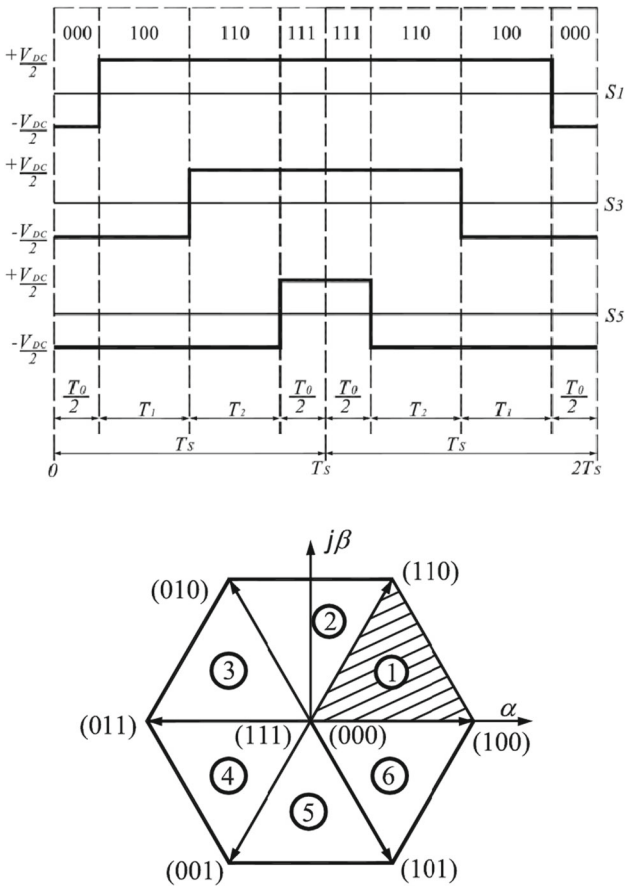

Fig. 5 Switching logic signals for Sector-I

Space vector modulation is a sophisticated PWM method that provides advantages such as higher DC bus voltage utilization and lower total harmonic distortion [15–18]. In SVM, three phase stationary reference frame voltages for each inverter switching state are mapped to the complex two phase orthogonal α–β plane. The mathematical transform for converting the stationary three phase parameters to the

orthogonal plane is known as the Clarke's transformation. The reference voltage is generated by two adjacent non-zero vectors and two zero vectors. The symmetry in the output waveforms are mainly responsible for having lower total harmonic distortion in SVM compared to SPWM in linear operating region. An arbitrary target output voltage vector, V_{ref}, is formed by the summation of a number of these space vectors within one switching period, which is shown in Fig. 4.

A typical seven segment switching sequence for generating reference vector in Sector-1 is shown in Fig. 5.

4 Field weakening control of induction machine

Maximum mechanical speed adjusted by the induction machine is limited by DC link voltage and PWM inverter strategy and the maximum current to an induction machine is decided by the thermal limit of the inverter or the machine itself. Field weakening is used to allow operation of variable speed induction motor drives at high speeds where the rotor flux is getting reduced to below its rated value [19]. In field-weakening control, d- and q-axis voltage references are used and the maximum phase voltage, V_{sm}, is decided by the DC link voltage V_{DC}, of the SVM inverter. For space vector modulation V_{sm} is obtained in the linear control range as $V_{\text{DC}}/\sqrt{3}$. The constraints can be simultaneously depicted in the voltage plane or in the current plane using the stator voltage equations of an induction machine. The reference current, I_{sm}, should satisfy (6) regardless of the reference frame.

$$I_{\text{sm}}^2 \geq i_{\text{sd}}^2 + i_{\text{sq}}^2 \tag{6}$$

The induction machine can generate the maximum torque at the field weakening region under a given voltage limit, which should satisfy the equation as:

$$V_{\text{sm}}^2 \geq V_{\text{sd}}^2 + V_{\text{sq}}^2 \tag{7}$$

In FW region, voltage limit ellipse can be obtained by neglecting current variations in the stator voltage equations and the voltage drop due to the stator resistance as:

$$(i_{\text{sd}}\omega_{\text{e}}L_{\text{s}})^2 + (i_{\text{sq}}\omega_{\text{e}}\sigma L_{\text{s}})^2 \leq V_{\text{sm}}^2, \tag{8}$$

whereω_{e} rotor flux speed; σ rotor leakage factor.

In constant torque region, stator flux magnitude is constant and the rotor speed is less than the rated speed. The base speed, ω_{b}, where the constant torque region ends is deduced as:

$$\omega_{\text{b}} = \sqrt{\frac{(V_{\text{sm}}/L_{\text{s}})^2}{[(\sigma I_{\text{sm}})^2 - (\sigma^2 - 1)i_{\text{sd}}^2]}} \tag{9}$$

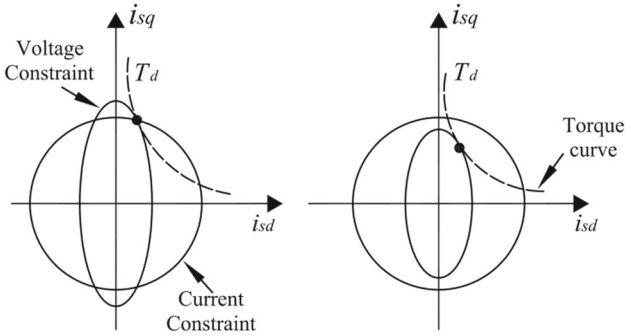

Fig. 6 Voltage constraint ellipse, current constraint circle, and torque locus

As the speed increases output power increases, when the applied voltage is at the maximum value, output power starts to decrease, the rate of decrease of developed power is related to drive parameters. Constant power region begins at base speed and ends at the speed where current limit is unattainable due to the voltage limit. To achieve speed higher than base speed, flux weakening algorithm has to be applied. The speed, where this region ends is deduced as:

$$\omega_1 = \frac{V_{\text{sm}}}{\sigma L_{\text{s}} I_{\text{sm}}}\sqrt{\frac{(1+\sigma^2)}{2}}. \tag{10}$$

If the operating frequency of the induction motor further increases from the field weakening region I and the ellipse shrinks further then the ellipse would be fully inside the circle. This operating region is referred to constant slip frequency region or characteristic region of the induction machine. There is no crossing point of ellipse and circle in this region and the torque is limited only by the voltage constraint. In this constant slip frequency region, the voltage limit is superseding the current limit and making a reduction in current.

The size of the voltage constraint ellipse decreases as the operating speed increases and current constraint can be represented as a circle in the current plane. The leakage factor of machine has influence on the area of ellipse at a specific frequency. Figure 6 shows the voltage constraint ellipse, current constraint circle, and torque locus.

5 Design modification of induction motor for maximum torque production

Existing constraints for the operation at field weakening are the maximum output voltage and the permitted maximum current of the inverter. To produce the maximum torque that the machine could possibly develop, the excitation level of field weakening must be appropriately adjusted. Most commonly used methods of excitation control do not fully utilize

the installed inverter power which can lead to a reduction of torque and power down to 65%. The innovative approach proposed in this paper is to carry out appropriate design modification of the induction motor by varying the rated value of power factor so as to explore maximum torque and power compared to its rated values.

The main specifications for the design of a three phase squirrel cage induction motor are: rated output power in HP or kW, frequency in Hz, voltage in volts, speed in rpm, efficiency, power factor, and full load current in ampere. The stator and rotor dimensions are determined by independent variables which are: stator slot height, stator tooth width, rotor slot height, rotor tooth width, air-gap length, air gap flux density, stack length, outer stator diameter, stator wire size, and electrical steel type. Besides the above independent variables, the design involves some non-linear constraints which concern mainly the motor performances.

Based on the standard design procedure, design spread sheets are developed for three phase squirrel cage induction machine. Design models are done for two cases namely Case-1 and Case-2 for 10 and 20 kW, respectively. Design options are generated by reducing the rated values of power factors and the options are named as Design-A, Design-B, Design-C, and Design-D for power factors equal to 0.9, 0.8, 0.7, and 0.6, respectively. The design values obtained from the design sheet for the above design options are tabulated and presented in Tables 4 and 5 for Cases-1 and 2, respectively, in the Appendix.

6 Simulation

The Simulink/MATLAB model for FOC induction machine with sensor using SVM inverter is developed in [20]. The above model is extended from base speed region to FW region in [21–25]. The simulation models for FOC induction machine with sensor is based on the block diagram which is shown in Fig. 7. For comparing the performance of the design options, Design-A, Design-B, Design-C, and Design-D, simulations are carried out for these design options using the above model.

In the simulation, the motor starts from a standstill state in no load condition and the speed responses are shown in Fig. 8. From the results, it is clear that the rotor speed increases from Design-A to Design-D, which means the rotor speed increases with the reduction in power factor. The maximum attainable speed at 8 seconds after starting the machine, is increased from Design-A to Design-D in both cases as given in Table 1.

Figure 9 shows the variation of electromagnetic torque (p.u.) with respect to rotor speed (p.u.) for various design options. Torque capability is improved in the FW region as the power factor decreases is demonstrated in Table 2.

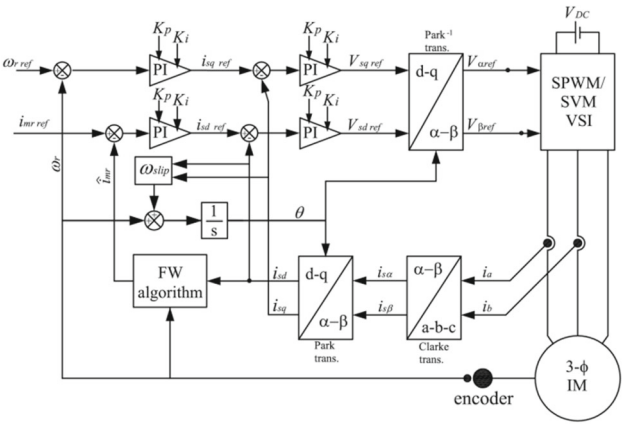

Fig. 7 Block diagram of FOC induction machine with sensor in FW region

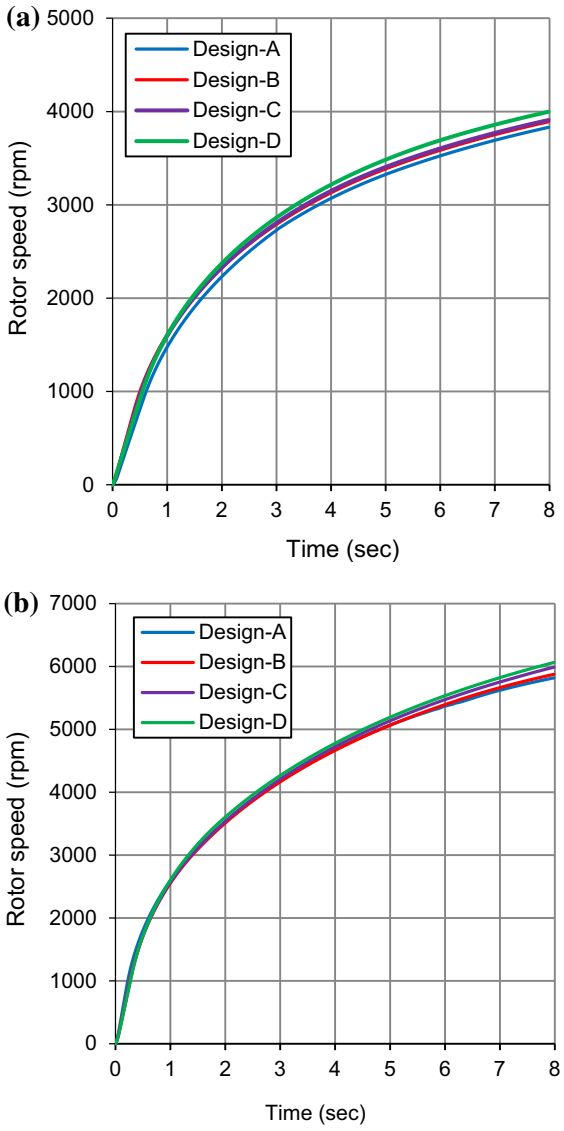

Fig. 8 Rotor speed vs. Time. **a** Case-1 (for 10 kW). **b** Case-2 (for 20 kW)

Table 1 Speed response (at 8 s)

Design options	ω_r (rpm)	
	Case-1	Case-2
Design-A	3830	5818
Design-B	3890	5819
Design-C	3909	5987
Design-D	4003	6062

Table 2 Torque capability (p.u.)

Design options	ω_r = 2.0 p.u.		ω_r = 3.0 p.u.	
	Case-1	Case-2	Case-1	Case-2
Design-A	0.371	0.401	0.231	0.232
Design-B	0.398	0.423	0.248	0.246
Design-C	0.411	0.445	0.255	0.267
Design-D	0.442	0.471	0.271	0.285

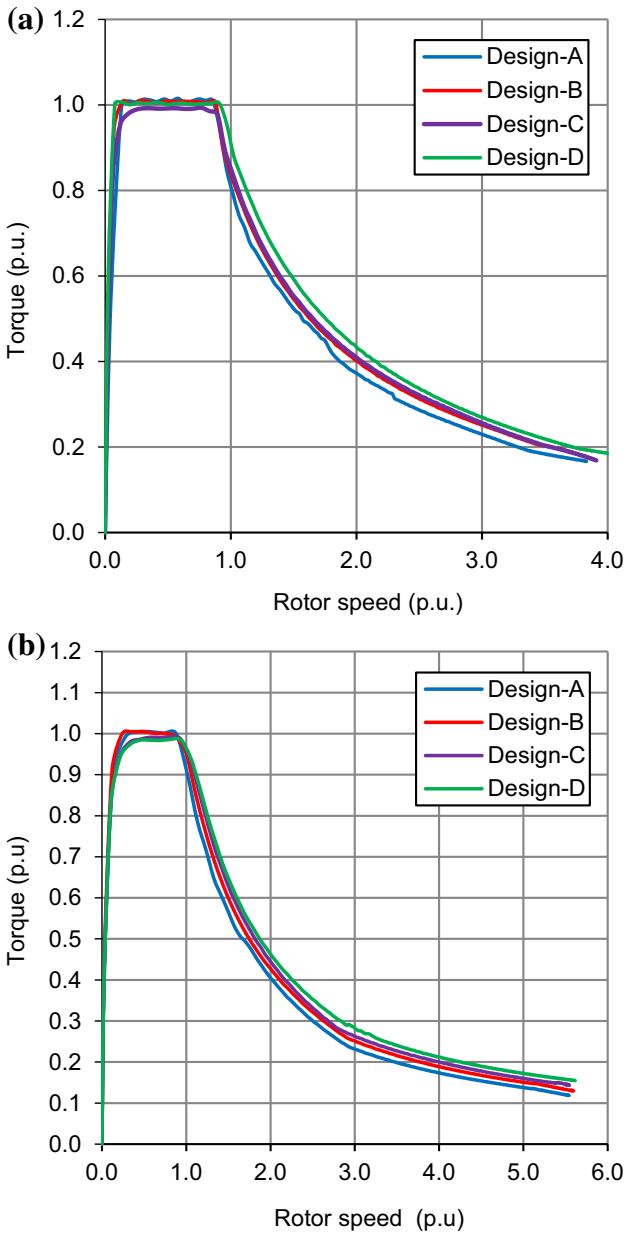

Fig. 9 Torque vs. Rotor speed. **a** Case-1 (for 10 kW). **b** Case-1 (for 20 kW)

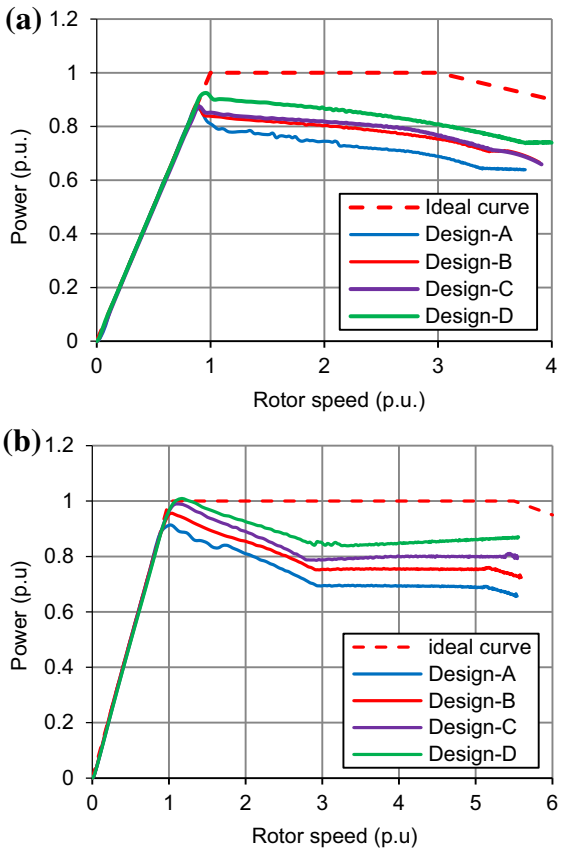

Fig. 10 Power vs. Rotor speed. **a** Case-1 (for 10 kW). **b** Case-2 (for 20 kW)

Variation of power (p.u.) with respect to rotor speed (p.u.) is presented in Fig. 10 for the design options. In the constant power region of the FW range, power increases from Design-A to Design-D, which implies that power increases with the reduction in power factor.

Table 3 shows that increase of power for Design-D compared to Design-A is about 17 and 22% in Cases 1 and 2, respectively, for rotor speed of 3.0 p.u.

Table 3 Maximum power (p.u.)

Design options	$\omega_r = 2.0$ p.u.		$\omega_r = 3.0$ p.u.	
	Case-1	Case-2	Case-1	Case-2
Design-A	0.742	0.802	0.693	0.696
Design-B	0.796	0.846	0.744	0.735
Design-C	0.822	0.890	0.765	0.801
Design-D	0.884	0.942	0.813	0.855

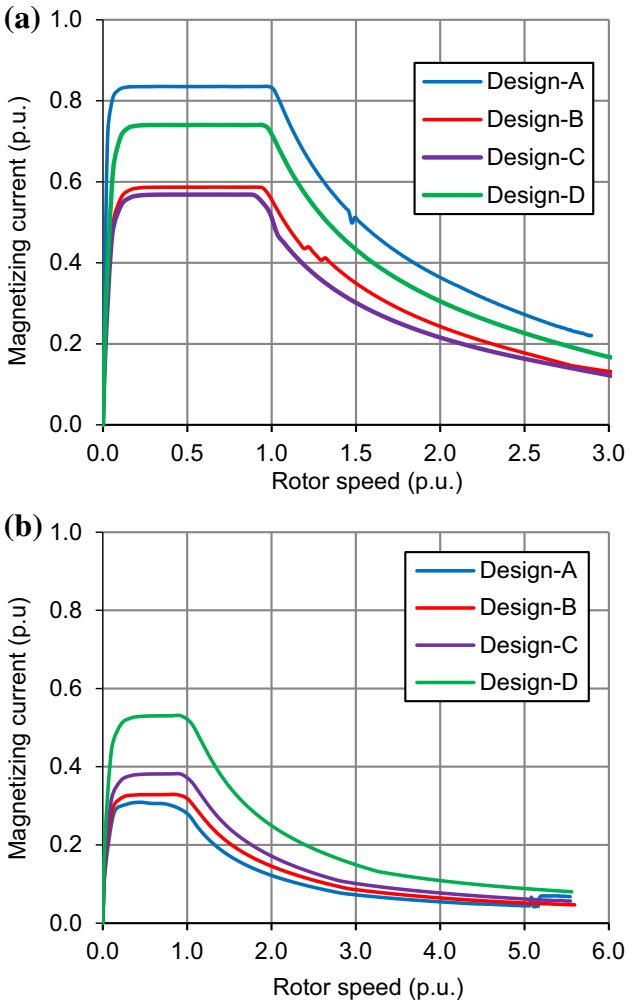

Fig. 11 Magnetizing current vs. Rotor speed. **a** Case-1 (for 10 kW). **b** Case-1 (for 20 kW)

The variation of rotor magnetizing current (p.u.) with respect to rotor speed (p.u.) is shown in Fig. 11. The magnetizing current curves for various design options are dissimilar in the entire speed range.

By observing the simulation results, it ensures that improvement of torque capability and power in FW region is possible by decreasing the power factor.

7 Conclusions

The original contribution in this paper is an innovative approach to improve the torque capability of induction machine in FW region by varying machine parameters rather than the conventional approach of maximizing the DC link voltage. MATLAB/Simulink simulation models for field oriented controlled induction machine with sensor using SVM inverter is used to operate various design options of induction machine for comparing the Torque-speed characteristics.

The maximum attainable rotor speed and torque capability of FOC induction machine in FW region is improved by decreasing the power factor of the induction machine from rated value. The maximum rotor speed attainable is increased when the power factor is reduced. Toque capability is improved by 15–20% in FW region, when the power factor is reduced by 33%. Constant power in FW region is increased by 20% when the power factor is reduced by 33%.

In future work, the proposed approach may be applied to sensorless operation of induction machine. Also, the robustness of the findings can be further investigated by hardware implementations and by generating the experimental results for ensuring the effectiveness of the proposed approach.

Acknowledgements The first author acknowledges support from SPEED-IT Research Fellowship from IT Department of the Government of Kerala.

8 Appendix

See Tables 4 and 5.

Table 4 Machine parameters of design options for Case-1 (for 10 kW)

Parameters		Design options				Unit
		A	*B*	*C*	*D*	
Full load output	P	10.0	10.0	10.0	10.0	kW
Line voltage	V	220	220	220	220	volts
Full load current	I_L	48.6	41.6	36.4	32.4	A
Synchronous speed	N_s	1500	1500	1500	1500	rpm
Rated torque	T_d	65	65	65	65	N-m
Frequency	f	50	50	50	50	Hz
No. of poles	Pole	4	4	4	4	
Power factor	pf	0.6	0.7	0.8	0.9	
Efficiency	η	86.1	87.6	88.5	89.4	%
Stator bore	D	210	200	190	195	mm
Core length	L	165	155	150	145	mm
Air gap length	l_g	0.57	0.55	0.54	0.53	mm
Dia. of conductors		2.12	2.06	1.90	1.80	mm
No. of turns/phase	T_s	86	96	106	112	Nos.
Diameter of rotor	D_r	209	199	189	184	mm

Table 4 continued

Parameters		Design options				Unit
		A	*B*	*C*	*D*	
Area of rotor bar	A_{br}	45	54	54	60	mm^2
Magnetizing current	i_{mr}	40.9	31.2	21.48	18.47	A

Table 5 Machine parameters of design options for Case-2 (for 20 kW)

Parameters		Design options				Unit
		A	*B*	*C*	*D*	
Full load output	P	20.0	20.0	20.0	20.0	kW
Line voltage	V	220	220	220	220	volts
Full load current	I_L	97.1	83.3	72.9	64.8	A
Synchronous speed	N_s	1500	1500	1500	1500	rpm
Rated torque	T_d	130	130	130	130	N-m
Frequency	f	50	50	50	50	Hz
No. of poles	Pole	4	4	4	4	
Power factor	pf	0.6	0.7	0.8	0.9	
Efficiency	η	86.1	87.6	88.5	89.4	%
Stator bore	D	265	250	240	230	mm
Core length	L	210	195	190	180	mm
Air gap length	l_g	0.67	0.64	0.63	0.61	mm
Dia. of conductors		2.65	2.50	2.36	2.24	mm
No. of turns/phase	T_s	54	62	66	72	Nos.
Diameter of rotor	D_r	264	249	239	229	mm
Area of rotor bar	A_{br}	60	66	70	77	mm^2
Magnetizing current	i_{mr}	52.43	32.4	25.5	21.38	A

References

1. Zeraoulia M, Benbouzid MEH, Diallo D (2006) Electric motor drive selection issues for HEV propulsion systems: a comparative study. IEEE Trans Veh Technol 55(6):1756–1764
2. Rub HA, Iqbal A, Guzinski J (2012) High performance control of AC drives. Wiley, New York, pp 375–388
3. Kim SH, Sul SK (1995) Maximum torque control of an induction machine in the field weakening region. IEEE Trans Ind Appl 31(4):787–794
4. Shin MH, Hyun DS, Cho SB (2002) Maximum torque control of stator flux oriented induction machine drive in the field weakening region. IEEE Trans Ind Appl 38(1):117–122
5. Bunte A, Grotstollen H, Krafka P (1996) Field weakening of induction motors in a very wide region with regard to parameter uncertainties. In: Proceedings of IEEE power electronics specialists conference PESC, June 1996, pp 944–950
6. Kim SH, Sul SK (1997) Voltage control strategy for maximum torque operation of an induction machine in the field weakening region. IEEE Trans Ind Appl 44(4):512–518
7. Harnefors L, Pietilanen K, Gertmar L (2001) Torque-maximizing field weakening control: design, analysis and parameter selection. IEEE Trans Ind Electron 48(1):161–168
8. Mengoni M, Zari L, Tani A, Serra G, Casadei D (2008) Stator flux vector control of induction motor drive in the field weakening region. IEEE Trans Power Electron 23(2):941–949
9. Lin PY, Lai YS (2011) Novel voltage trajectory control for field-weakening operation of induction motor drives. IEEE Trans Ind Appl 47(1):122–127
10. Levi E, Wang M (2002) A speed estimator for high performance sensorless control of induction motors in the field weakening region. IEEE Trans Power Electron 17(3):365–378
11. Leonhard W (1996) Control of electrical drives. Springer, New York, pp 163–180
12. Lakaparampil ZV, Fathima KA, Ranganathan VT (1996) Design modeling simulation and implementation of vector controlled induction motor drive. Proc Power Electron Drive Syst 2:862–868
13. Nisha GK, Lakaparampil ZV, Ushakumari S (2012) Sensorless vector control of SVPWM fed induction machine using MRAS—sliding mode. In: Proceedings of IEEE international conference on green technology, ICGT 2012, December 2012, pp 29–36
14. Holmes DG, Lipo TA (2003) Pulse width modulation for power converters: principles and practice. Wiley IEEE Press, New Jersey
15. Nisha GK, Ushakumari S, Lakaparampil ZV (2012) Method to eliminate harmonics in PWM: a study for single phase and three phase. In: Proceedings of international conference on emerging technology trends on advanced engineering research, ICETT 2012, Kollam, India, February 2012, pp 598–604
16. Nisha GK, Ushakumari S, Lakaparampil ZV (2012) Harmonic elimination of space vector modulated three phase inverter. Lecture notes in engineering and computer science. In: Proceedings of the international multi-conference of engineers and computer scientists 2012, March 2012, pp 1109–1115
17. Nisha GK, Ushakumari S, Lakaparampil ZV (2012) CFT based optimal PWM strategy for three phase inverter. In: Proceedings of IEEE international conference on power, control and embedded systems. ICPCES 2012, December 2012, pp 1–6
18. Nisha GK, Ushakumari S, Lakaparampil ZV (2012) Online harmonic elimination of SVPWM for three phase inverter and a systematic method for practical implementation. IAENG Int J Comput Sci 39(2):220–230
19. Sul S-K (2011) Control of electric machine drive systems. Wiley, New Jersey, pp 255–267
20. Nisha GK, Lakaparampil ZV, Ushakumari S (2013) FFT analysis for field oriented control of SPWM and SVPWM inverter fed induction machine with and without sensor. Int J Adv Electr Eng 2(4):151–160
21. Nisha GK, Lakaparampil ZV, Ushakumari S (2013) Sensorless field oriented control of SVM inverter fed induction machine in field weakening region using sliding mode observer. Lecture notes in engineering and computer science. In: Proceedings of the 7th world congress on engineering, London, July 2013, pp 1174–1181
22. Nisha GK, Lakaparampil ZV, Ushakumari S (2013) Performance study of field oriented controlled induction machine in field weakening using SPWM and SVM fed inverters. Int Rev Model Simul 6(3):741–752
23. Nisha GK, Lakaparampil ZV, Ushakumari S (2013) Four quadrant operation of sensorless FOC induction machine in field weakening region using MRAS—sliding mode observer. In: Proceedings of IEEE international conference on control communication and computing, ICCC, Trivandrum, India, December 2013, pp 33–38
24. Nisha GK, Lakaparampil ZV, Ushakumari S (2014) Effect of leakage inductance on torque capability of field oriented controlled induction machine in field weakening region. In: International conference on advances in engineering and technology ICAET, March 2014, pp 741–752
25. Nisha GK, Lakaparampil ZV, Ushakumari S (2014) Four quadrant operation of field weakened FOC induction motor drive using sliding mode observer. In: Transactions on engineering technologies, Springer publication, May 2014, special volume of WCE, pp 385–402